PHYSICAL REVIEW RESEARCH **3**, 033046 (2021)

Superstructures arising from V trimers with orbital ordering in $BaV_{10}O_{15}$

Tomomasa Kajita,[1] Hideki Kuwahara,[2] Shigeo Mori,[3] and Takuro Katsufuji[1,4]
[1]*Department of Physics, Waseda University, Tokyo 169-8555, Japan*
[2]*Department of Physics, Sophia University, Tokyo 169-8555, Japan*
[3]*Department of Materials Science, Osaka Prefecture University, Sakai 599-8531, Japan*
[4]*Kagami Memorial Research Institute for Materials Science and Technology, Waseda University, Tokyo 169-0051, Japan*

(Received 12 April 2021; accepted 23 June 2021; published 12 July 2021)

In $BaV_{10}O_{15}$ with quasitriangular V lattices, we found unique superstructures characterized by $(qq0)$-type peaks in the momentum space, where q varies continuously with temperature between $q = 0$ and $1/3$ and locks at $1/3$. Such a threefold superstructure is likely caused by the dense arrangement of the V trimers associated with the orbital ordering of V. The results indicate that the superstructure of the V trimers, each of which is also a superstructure, gives rise to the ordered phases with peculiar characteristics.

DOI: 10.1103/PhysRevResearch.3.033046

I. INTRODUCTION

In crystals, superstructures of charge or spin with a period longer than that of the underlying lattice are often observed. For example, superstructures of charge are found in charge-density-wave (CDW) states [1–7] and charge-ordered (CO) states [8–10], and superstructures of spin are found in spin-density-wave (SDW) states [11] and helical magnetic states [12,13]. The period of these superstructures is dominated by the nesting vector of the Fermi surface, the number of carriers, or the magnitude ratio of two interactions, and can be a noninteger multiple of the lattice period, called incommensurate structures. In some cases, the period of these superstructures exhibits a temperature (T) dependence, but in most cases, it is a discontinuous change with T or a continuous change with T in a range of wave number q that is much smaller than the size of the Brillouin zone.

It is known that the orbital degree of freedom that arises from localized d electrons in transition-metal compounds also exhibits ordering, called orbital ordering. In this orbital-ordered (OO) state, specific states among the energetically degenerate orbitals are occupied by electrons at each site. Such an OO state has been observed in various transition-metal oxides, for example, manganites [14,15], titanates [16,17], vanadates [18–23], cuprates [24], ruthenates [25–27], and molybdenites [28]. The periods of the orbital ordering in these materials are commensurate with the unit cell, and no incommensurate orbital ordering has been reported so far, except for that of manganites, where OO and CO coexist [15].

$BaV_{10}O_{15}$ is known to exhibit an OO state below ~130 K [29–35]. In this compound, the average valence of the V ions is +2.8, which means that, nominally, there are one V^{2+} ($3d^3$) ion and four V^{3+} ($3d^2$) ions per five V ions. The V^{3+} ion, which has two electrons in the triply degenerate t_{2g} orbitals, has the orbital degree of freedom. This compound takes an orthorhombic crystal structure (the space group *Cmce*) and is characterized by a 5 V boat-shaped cluster connected along the *ab* plane, as shown in Fig. 1(a). The arrangement of the V ions thus constructed can be regarded as a triangular lattice from which triangles are periodically missing [shown by dashed circles in Fig. 1(a)]. Two layers of such quasitriangular lattices have opposite directions of the boats, as shown in Fig. 1(b), and are the building unit of this compound. The V ion is surrounded by six oxygen ions in the octahedral configuration, and all the VO_6 octahedra share an edge with each other within this bilayer.

This compound exhibits a structural phase transition from *Cmce* to *Pbca* at $T_s \sim 130$ K. Below T_s, the three V ions existing at the corners of a nearly regular triangle spanning the bilayers approach each other to form a V trimer, as shown by the yellow color in Fig. 1(c). Note that not all the V ions in the crystal form trimers but some of them remain as lone V ions. According to the results of resonant x-ray scattering [35], a σ bond of one of the t_{2g} orbitals (xy, yx, or zx) between the neighboring V ions is formed at each edge of the trimer below T_s, as shown in Fig. 2(a). A similar V trimerization has been observed in various vanadates, for example, $LiVO_2$ [18,19], $Ba_2V_{13}O_{22}$ [21], and $BaV_{13}O_{18}$ [23], and similar bond-order-type orbital ordering has been observed in various compounds such as $NaTiSi_2O_6$ [16,17], AlV_2O_4 [20,22], Li_2RuO_3 [27], and $LiA_2Mo_3O_8$ [28]. Upon the orbital ordering with the structural phase transition at T_s, the electrical resistivity jumps by three orders of magnitude and other properties also markedly change in $BaV_{10}O_{15}$ [33].

The arrangement of the V trimers in $BaV_{10}O_{15}$ can be understood easily as follows. If the center V ion is removed from the 5 V boat, the remaining V ions are arranged along the *b* axis in the crystal as a zigzag double chain, as shown within the solid lines in Figs. 1(b) and 1(c). In this V double chain,

---

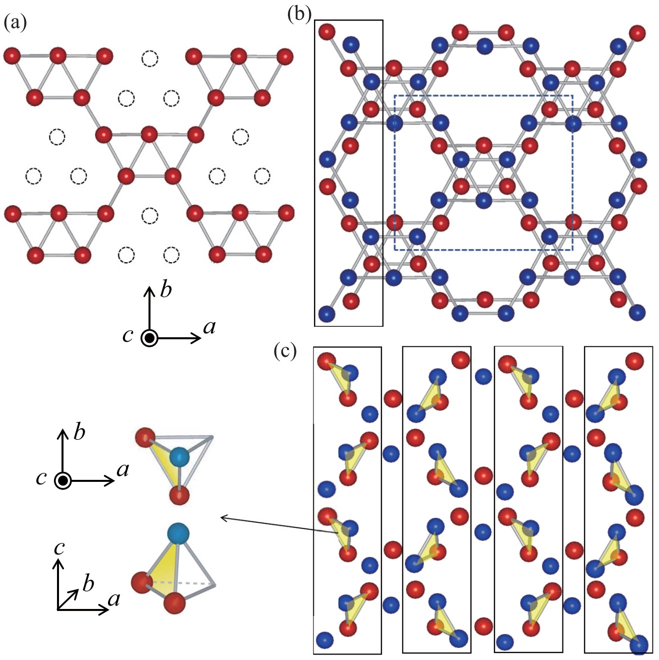

FIG. 1. Arrangement of the V ions in $BaV_{10}O_{15}$ along the *ab* plane for (a) one layer above T_s, (b) two layers (red and blue for each layer) above T_s, and (c) two layers below T_s. Figures were drawn using VESTA [36]. The yellow triangles in (c) represent the V trimers. The dashed-line rectangle in (b) indicates the unit cell. The solid-line rectangles in (b) and (c) indicate the zigzag double chains of V.

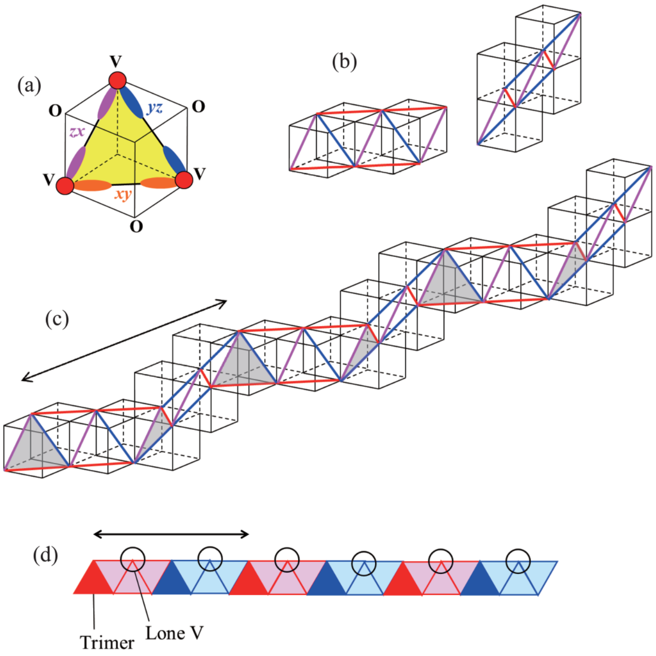

FIG. 2. (a) Orbital states (σ bonds of the t_{2g} orbitals *xy*, *yz*, *zx*) in the V trimer for $BaV_{10}O_{15}$. (b) Two units of the V double chain in a parallelogram, each of which is composed of four V triangles. V ions exist on the corners of the triangles. Three different colors (red, blue, and magenta) of the edges depict the bonds composed of three different t_{2g} orbitals: *xy*, *yx*, and *zx* shown in (a). (c) V double chain with V trimerization. The shaded triangle corresponds to a V trimer, and the corner that does not belong to the shaded triangle corresponds to the lone V ion. (d) Flattened picture of the V double chain. Different colors (red and blue) correspond to the two types of parallelogram with different normal vectors shown in (b) and (c). The arrows in (c) and (d) indicate the period of the structure.

four V triangles on the same plane form a parallelogram, as shown by red, blue, and magenta lines in Fig. 2(b), and are connected in a zigzag manner by sharing edges with each other, as shown in Fig. 2(c) (note that the V ions exist at the vertices of the triangles). The four V triangles on the same plane can be regarded as that within four cubes consisting of V and O, as shown by black lines in Figs. 2(b) and 2(c). The V trimerization occurs at one of the four triangles in each parallelogram, while the remaining vertex corresponds to the lone V, as shown in Fig. 2(c). Note that there are four V ions in each parallelogram, considering the fact that they share two V ions on each side, and they are divided into a V trimer and a lone V below T_s.

This description can be further simplified by flattening the zigzag plane and drawing two planes originally having different normal vectors newly on the same plane in red and blue, as shown in Fig. 2(d). These illustrations clarify that the presence of the lone V in the ordered phase is the unavoidable consequence to make the superstructure of V trimers commensurate with the period of the lattice shown by the arrow in Fig. 2(d).

Here, we point out that, in addition to the phase transition at T_s, anomalies above T_s are suggested in some experiments for $BaV_{10}O_{15}$: ^{51}V NMR indicates that some V sites become inequivalent below 220 K [34], and the Seebeck coefficient starts to increase below ~200 K [37]. These results imply the existence of other phases above the OO phase. It is known that some transition-metal compounds exhibit two or more different types of ordering with T [23,38,39]. In the present study, we investigated various properties of $BaV_{10}O_{15}$ above T_s using single crystals and found that various intermediate-temperature phases appear above T_s and are possibly dominated by the V trimers similarly to the ordered state below T_s but in different arrangements.

II. EXPERIMENT

The single crystals of $BaV_{10}O_{15}$ were grown by the floating-zone method in a reducing atmosphere. In this study, the single crystal with $T_s = 135$ K, which is higher than that used in the previous study ($T_s = 123$ K) [33], was mainly used. The crystal axes were determined by the x-ray Laue method. The electrical resistivity was measured by a standard four-probe method. Magnetic susceptibility was measured with a SQUID magnetometer. The strain of the crystal was measured by a strain-gauge technique. The x-ray diffraction images of the single crystal were taken using a Rigaku diffractometer (Rapid-II) with Cu Kα radiation equipped with an imaging plate under variation of T with N_2 gas flow. The electron diffraction experiments were carried out with a JEM-2010 transmission electron microscope. The specific heat was measured by a thermal relaxation method using physical property measurement systems (PPMS).

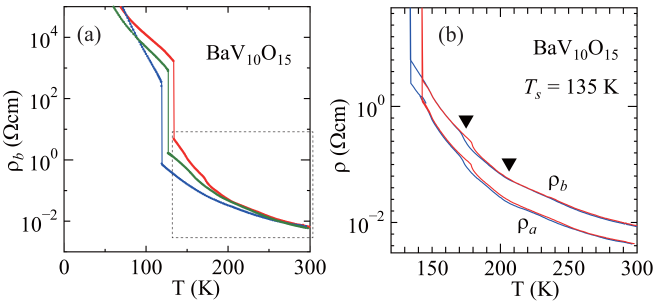

FIG. 3. (a) Resistivity along the b axis for $BaV_{10}O_{15}$ with $T_s =$ 135 K (red), 128 K (green) and 123 K (blue). (b) Enlarged figure of the resistivity above T_s along the a and b axes for the sample with $T_s = 135$ K. The blue and red lines correspond to the data in the cooling and warming runs, respectively. The dashed-line rectangle in (a) corresponds to the drawing range of (b).

III. RESULTS

Figure 3(a) shows the T dependence of the resistivity along the b axis (ρ_b) for the sample with $T_s = 123$ K, 128 K, and 135 K. Although the absolute values of ρ_b are comparable at 300 K, with decreasing T, ρ_b for the samples with $T_s = 135$ and 128 K starts to become larger than that with $T_s = 123$ K at ~200 K, and ρ_b for the sample with $T_s = 135$ K becomes almost one order of magnitude larger than that with $T_s = 123$ K immediately above $T_s = 135$ K. In addition to a large jump in the resistivity at T_s existing in all the samples, a small anomaly is observed for the sample with $T_s = 135$ K at $T \sim 175$ K. This is more clearly seen in the enlarged figure for the sample with $T_s = 135$ K in Fig. 3(b); both the resistivity along the a axis [$\rho_a(T)$] and $\rho_b(T)$ increase at ~175 K with decreasing T with T hysteresis, as shown by a triangle. Such an anomaly is barely observed for the sample with $T_s = 128$ K and is absent for the sample with $T_s = 123$ K.

Similar anomalies above T_s are observed also in the T dependence of the magnetic susceptibility $\chi(T)$. Namely, as shown in Fig. 4(a), in addition to a large jump at T_s, small anomalies are clearly observed at 175 K and 205 K for the sample with $T_s = 135$ K. Similar anomalies are observed for the sample with $T_s = 128$ K but at lower T, whereas they are almost absent for the sample with $T_s = 123$ K. As shown in Fig. 4(b), these anomalies can be observed for the magnetic susceptibility with all the directions of the magnetic field (χ_a, χ_b, and χ_c), and the anomaly at $T = 175$ K has T hysteresis.

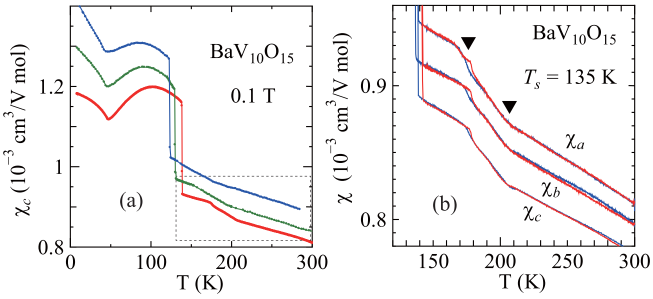

FIG. 4. (a) Magnetic susceptibility with the magnetic field of 0.1 T applied along the c axis for $BaV_{10}O_{15}$ with $T_s = 135$ K (red), 128 K (green), and $T_s = 123$ K (blue). (b) Enlarged figure of the magnetic susceptibility above T_s along the a, b, and c axes for the sample with $T_s = 135$ K. The three data sets are offset for clarity. The blue and red lines correspond to the data in the cooling and warming runs, respectively. The dashed-line rectangle in (a) corresponds to the drawing range of (b).

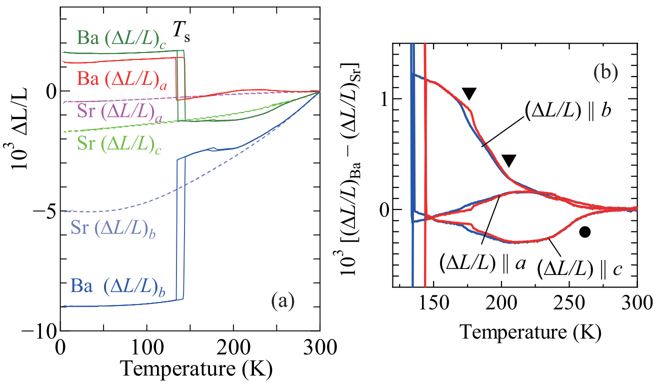

FIG. 5. (a) Strain along the a, b, and c axes for $BaV_{10}O_{15}$ with $T_s = 135$ K (solid lines) and $SrV_{10}O_{15}$ (dashed lines). (b) Difference between strain for $BaV_{10}O_{15}$ and that for $SrV_{10}O_{15}$ above T_s along the a, b, and c axes. The blue and red lines correspond to the data in the cooling and warming runs, respectively.

The difference in the transition temperature T_s likely arises from the difference in the offstoichiometry of the sample, as reported in Ref. [30]. In the following, we mainly discuss the result of the sample with $T_s = 135$ K, which exhibits the anomalies most clearly.

To understand these anomalies from the structural point of view, strain was measured along the a [$(\Delta L/L)_a$], b [$(\Delta L/L)_b$], and c [$(\Delta L/L)_c$] directions for $BaV_{10}O_{15}$ with $T_s = 135$ K, together with $SrV_{10}O_{15}$, which does not exhibit any structural phase transition down to the lowest T [40]. As shown in Fig. 5(a), with decreasing T, $(\Delta L/L)_b$ decreases (shrinks) whereas $(\Delta L/L)_b$ and $(\Delta L/L)_c$ increase (expand) at T_s for $BaV_{10}O_{15}$. This is caused by the V trimerization associated with the orbital ordering, as discussed in the introduction. In addition to such a large change at T_s, $(\Delta L/L)_b$ decreases more than $(\Delta L/L)_a$ and $(\Delta L/L)_c$ with decreasing T even above T_s for both $BaV_{10}O_{15}$ and $SrV_{10}O_{15}$. We confirmed that such T dependence of the strain is quantitatively consistent with the T dependence of the lattice constants obtained by the x-ray diffraction described below. Such anisotropy in the T dependence of the strain or the lattice constants is caused by the evolution of orbital correlation along the b axis, as shown by the measurement of the strain dependence in the optical spectra for $BaV_{10}O_{15}$ [41].

Furthermore, small anomalies are observed in the strains above T_s. To see this more clearly, the difference between the strain for $BaV_{10}O_{15}$ and that for $SrV_{10}O_{15}$ is plotted in Fig. 5(b). As can be seen, anomalies at 175 K with T hysteresis and at 205 K can be observed for all directions; with decreasing T, the difference in the strain along the b axis increases substantially at both 205 K and 175 K, whereas that along the a axis slightly decreases and that along the c axis slightly increases at both 205 K and 175 K. It should also be

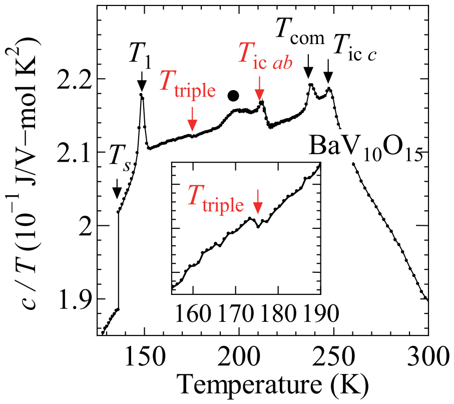

FIG. 6. Specific heat of $\mathrm{BaV_{10}O_{15}}$ with $T_s = 135$ K. The dots correspond to the experimental data and they are connected by a solid line for clarity. The inset is the enlargement around $T_{\mathrm{triple}} = 175$ K.

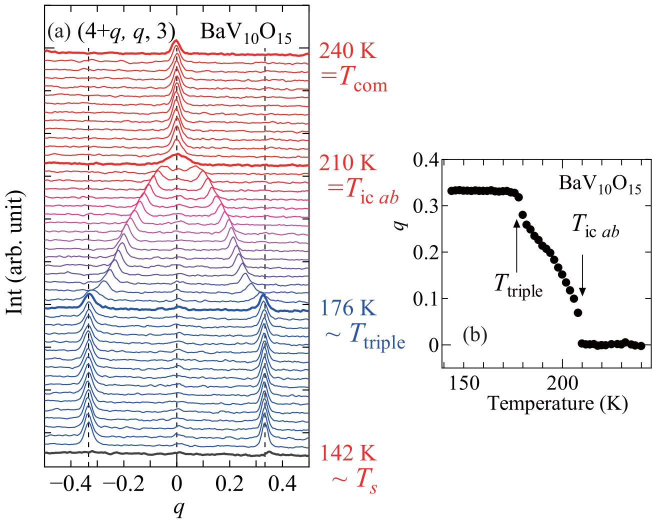

FIG. 7. (a) X-ray diffraction along $(4 + q, q, 3)$ for $\mathrm{BaV_{10}O_{15}}$ with decreasing T from 240 K to 142 K in 2 K steps (except for the data between 240 K and 220 K in 2.5 K steps). (b) T dependence of the position of the superlattice peak q.

pointed out that the difference in the strain along the c axis starts to decrease at ~260 K with decreasing T.

To find out all the phase transitions of $\mathrm{BaV_{10}O_{15}}$, specific heat was measured by a relaxation method. Figure 6 shows the specific heat c divided by T between 120 K and 300 K for $\mathrm{BaV_{10}O_{15}}$. Surprisingly, in addition to a sudden drop of c/T at T_s caused by the first-order phase transition, many peaks appear in this T range. Upon cooling from 300 K, two peaks successively appear at $T_{\mathrm{ic}\ c} = 250$ K and $T_{\mathrm{com}} = 240$ K. With further decrease in T, another peak appears at $T_{\mathrm{ic}\ ab} = 210$ K, followed by a broad peak at around 190 K and a small step at $T_{\mathrm{triple}} = 175$ K. (The meaning of the suffix will be described with the results of the x-ray diffraction below.) The anomalies at $T_{\mathrm{ic}\ ab} = 210$ K and $T_{\mathrm{triple}} = 175$ K correspond to the anomalies observed in the resistivity, magnetic susceptibility, and strain. The steplike structure in the specific heat at T_{triple} is consistent with the first-order phase transition with T hysteresis observed in the resistivity. Finally, another peak is observed at $T_1 = 150$ K before showing a step at $T_s = 135$ K. Note that the suppression of the entropy with each phase transition estimated from the integral of C/T with respect to T is the order of 10^{-1} J/V-mol K, which is much smaller than the gas constant $R \sim 8.31$ J/mol K multiplied by $\ln 2 \sim 0.69$ for the entropy of the $s = 1/2$ spin, for example, indicating that the suppression of the degrees of freedom at each phase transition is relatively small.

To reveal the structural change in $\mathrm{BaV_{10}O_{15}}$ above T_s, we performed single-crystal x-ray diffraction measurement from 300 K to 100 K. In the measurement, the images were taken by setting the incident x-ray beam along the ab plane of the crystal and by oscillating the crystal around the c axis by 10 degrees. First, let us see what happens at $T_{\mathrm{ic}\ ab} = 210$ K and $T_{\mathrm{triple}} = 175$ K. Figure 7(a) shows the x-ray diffraction along $(4 + q, q, 3)$ for $\mathrm{BaV_{10}O_{15}}$ at various T values. At 240 K, a peak is observed at (403) ($q = 0$), which is forbidden for the space group $Cmce$. This means that the c glide is broken at this T. This 403 peak remains down to 210 K but begins to split into the peaks at $(4 + q, q, 3)$ and $(4 - q, -q, 3)$ below $T_{\mathrm{ic}\ ab} = 210$ K. With further decrease in T, q continuously increases and is locked to $q = 1/3$ at $T_{\mathrm{triple}} = 175$ K. Figure 7(b) shows the T dependence of q. These results indicate that the phase transition at $T_{\mathrm{ic}\ ab} = 210$ K is the one from a commensurate to an incommensurate structure along the ab plane, and the phase transition at $T_{\mathrm{triple}} = 175$ K with T hysteresis corresponds to the commensurate locking to $q = 1/3$. The superlattice peaks at $(4 \pm 1/3, \pm 1/3, 3)$ remain down to 144 K but suddenly disappear at $T_s = 142$ K, where the structural phase transition to the low-T phase (space group $Pbca$) occurs.

This type of superstructure can also be observed in the electron diffraction. Figure 8 shows the electron diffraction patterns taken from the $[1\bar{1}0]$ direction. At 150 K, in addition to the fundamental spots, those dividing the span between the two fundamental spots along the (110) direction into three appear, corresponding to the $(4 \pm 1/3, \pm 1/3, 3)$ peaks observed in the x-ray diffraction. These spots disappear at 117 K $< T_s = 135$ K.

Regarding the phase transitions at $T_{\mathrm{ic}\ c} = 250$ K and $T_{\mathrm{com}} = 240$ K observed in the results of specific heat, we found that superlattice peaks at $(4, 0, 3 \pm q')$ ($q' \sim 0.1$) appear below $T_{\mathrm{ic}\ c} = 250$ K, and then, with decreasing T, q' approaches zero and the commensurate peak at (403) is established at $T_{\mathrm{com}} = 240$ K, as shown in Fig. 9. Namely, the phase transition at $T_{\mathrm{ic}\ c} = 250$ K is the one into an

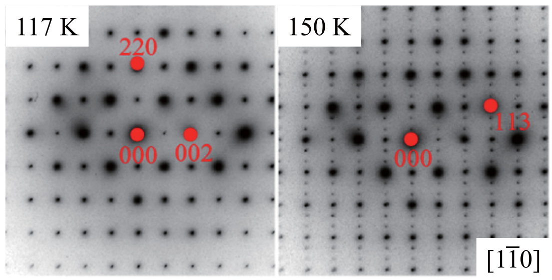

FIG. 8. Electron diffraction patterns of $\mathrm{BaV_{10}O_{15}}$ taken from the $[1\bar{1}0]$ direction at 150 K and 117 K.

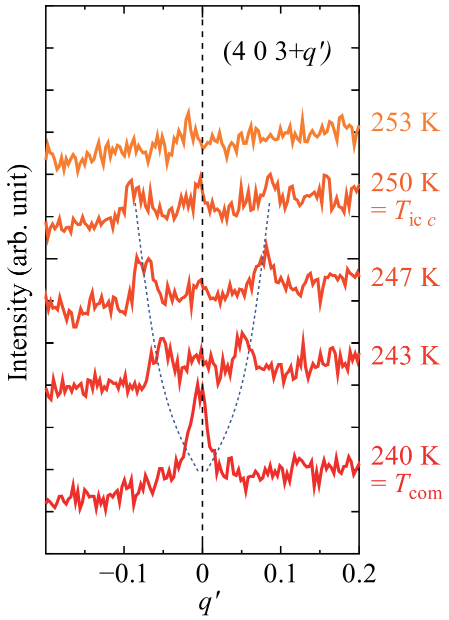

FIG. 9. X-ray diffraction along $(4, 0, 3 + q')$ for $\mathrm{BaV_{10}O_{15}}$ at various T values.

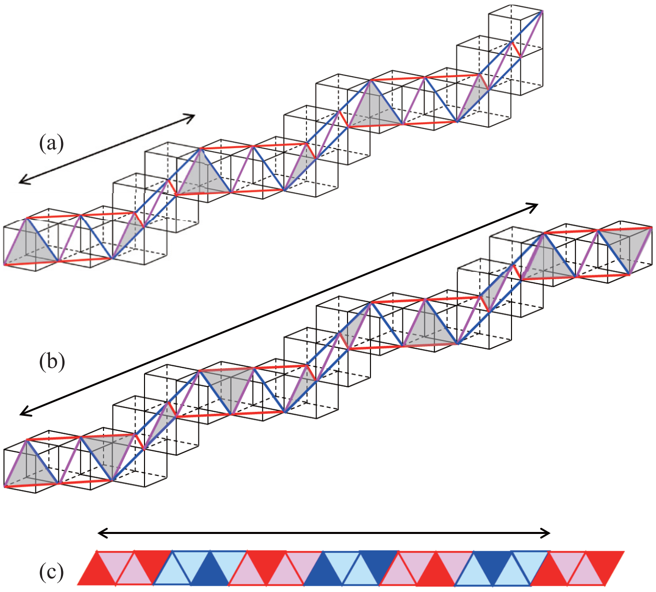

FIG. 10. Schematic pictures of the V trimers in the V double chain (a) with a commensurate structure for $T < T_s$, (b) with a threefold superstructure for $T_s < T < T_{\mathrm{triple}}$, and (c) the flattened picture for the threefold superstructure in (b). Each arrow indicates the period of the structure.

incommensurate structure along the c axis, and the phase transition at $T_{\mathrm{com}} = 240$ K is the one into a commensurate structure with $q = 0$. Note that the deviation of the strain along the c axis $(\Delta L/L)_c$ for $\mathrm{BaV_{10}O_{15}}$ from that for $\mathrm{SrV_{10}O_{15}}$ below 260 K shown in Fig. 5(b) can be related to the formation of such an incommensurate structure along the c axis.

In the present x-ray experiment, no anomaly related to the peak in the specific heat at $T_1 = 150$ K (Fig. 6) has been observed. This suggests that the phase transition at T_1 is of magnetic origin, although the details are yet to be clarified.

IV. DISCUSSION

Let us first discuss the origin of the threefold superstructure between $T_{\mathrm{triple}} = 175$ K and $T_s = 135$ K. It is known that such a superstructure can be caused by the modulation of charge density in the CDW state or CO state. In such states, the superstructure can be incommensurate with the lattice, similarly to the present case above T_{triple}. However, for $\mathrm{BaV_{10}O_{15}}$, the average number of d electrons per V ion is 2.2, and the number of V ions per unit cell is 10: If only the V ions in the double chain are considered, their number is 8. In any case, it is highly unlikely that these electrons in $\mathrm{BaV_{10}O_{15}}$ cause a threefold superstructure as the CO state.

Here, we remember that the alternate arrangement of V trimers and lone V below T_s is the constraint for the structure to be commensurate with the lattice [Fig. 10(a)]. If we make the V trimers as dense as possible along the double chain without lone V, their arrangement becomes incommensurate with the period of the lattice, and the positions of the trimer in the parallelogram changes for each successive period and return after three unit cells, as shown in Figs. 10(b) and 10(c). Namely, one unit consists of eight triangles, and trimerization every three triangles results in the period of three units (24 triangles). This can naturally explain the threefold superstructure experimentally observed for $T_s < T < T_{\mathrm{triple}}$.

Note that the superlattice peaks appear at $(h \pm 1/3, k \pm 1/3, l)$ experimentally and thus, the modulation exists not only along the b axis but also along the a axis. The pattern shown in Fig. 11 is one of the arrangements consistent with the superlattice peaks at $(h \pm 1/3, k \pm 1/3, l)$, where the position of the V trimers moves to the next triangle as it goes to the next double chain.

Let us also consider the origin of the $(h \pm q, k \pm q, l)$ peaks with $0 < q < 1/3$ between $T_{\mathrm{ic}\,ab} = 220$ K and $T_{\mathrm{triple}} =$

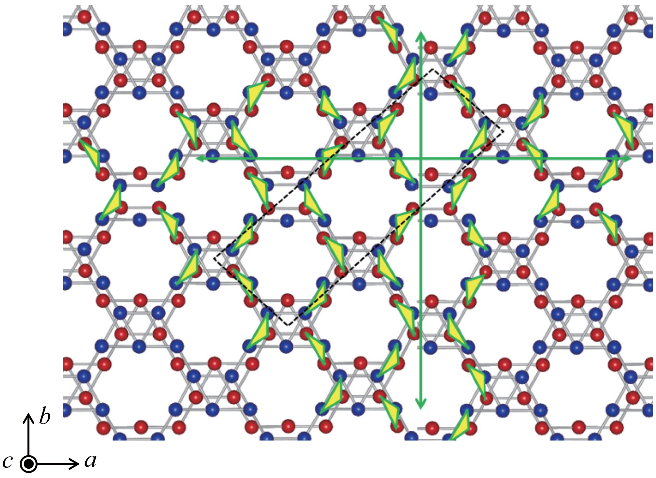

FIG. 11. Schematic of the V trimers (yellow triangles) along the ab plane, which is consistent with superlattice peaks at $(h \pm 1/3, k \pm 1/3, l)$ for $\mathrm{BaV_{10}O_{15}}$. The dashed rectangle represents a unit cell with the superstructure.

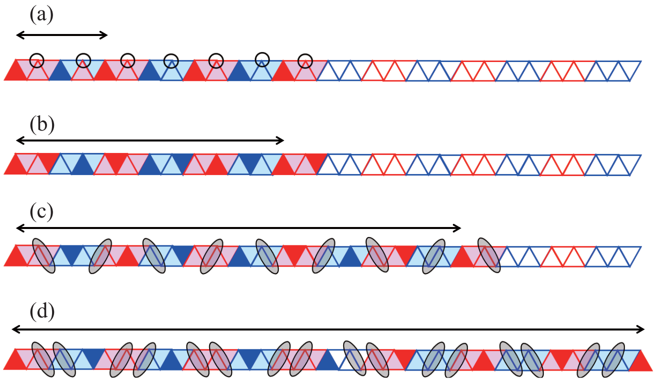

FIG. 12. Schematic of the V trimers in the V double chain in the flattened depiction for (a) a commensurate structure, (b) threefold superstructure, (c) fivefold superstructure, and (d) sevenfold superstructure. Each arrow indicates the period of the structure.

175 K shown in Fig. 7, corresponding to a period of the superstructure longer than three unit cells. As discussed in the introduction, the addition of a lone V between two trimers results in the commensurate structure, as observed below T_s [Fig. 12(a)]. In this case, the orientation of the neighboring triangles changes with the insertion of a lone V [Figs. 12(a) and 12(b)] and thus, the continuous change in the superstructure as observed experimentally is not possible. However, if a V dimer is inserted between two trimers, the structure remains incommensurate and the orientation of the neighboring triangles does not change. In this case, positions of the trimers in the parallelogram return after five unit cells, resulting in the fivefold superstructure shown in Fig. 12(c). If two dimers are inserted between two trimers, it produces the sevenfold superstructure shown in Fig. 12(d). In general, if n dimers are inserted between two trimers, trimers are formed every $(3 + 2n)$ triangles and the period becomes $(3 + 2n)$ times the unit consisting of eight triangles.

Indeed, an inflection point can be seen in the T dependence of q in Fig. 7(b) at ~190 K, where q is approximately $1/5$, and a broad peak is observed at that T in the specific heat, as shown by the solid circle in Fig. 6. This anomaly may correspond to the state with $q = 1/5$. Note that if only the hybridization by the direct transfer between the orbitals of neighboring V ions is considered, one dimer can accommodate only two electrons in the spin-singlet state and there will be one excess electron left on each V ion of the dimer. One possibility is that another orbital of the V ions in the dimer is also hybridized with each other, enabling two electrons to be accommodated per dimer. Another possibility is that hopping of the excess electrons occurs across the V ions throughout the entire crystal.

To explain the change in the q position of the superlattice peaks over one third of the Brillouin zone, namely, the change in the pattern of the orbital ordering from Figs. 12(d) to 12(b) with decreasing T, let us first consider the analogy to the transition from the incommensurate (IC) to the commensurate (C) CDW state, as observed in TaS_2, $TaSe_2$, and $NbSe_2$ [42–45]. In these compounds, the wave number q in the IC-CDW phase continuously changes with decreasing T and then exhibits a sudden change, corresponding to a transition into a C-CDW phase. This can be explained by the Landau theory, where the energy of the electronic part is the lowest in the IC-CDW state but the Umklapp term or the term called commensurability energy, which arises from the coupling with the lattice, induces a locking of the CDW to the lattice and thus, it stabilizes the C-CDW state. This model can reproduce the T-dependent q in the IC-CDW phase and the transition into the C-CDW phase [44,45]. Note that the superposition of the higher harmonics in the IC-CDW state, which leads to a discommensurate CDW state instead of a sinusoidal CDW state, plays an important role to reduce the energy of the IC-CDW phase.

However, it is not obvious if such a model can explain a large shift in the wave number of the superlattice peaks over one third of the Brillouin zone as observed in $BaV_{10}O_{15}$. Nevertheless, we see an analogy between the ordered state with $0 < q < 1/3$ in the present compound [shown in Figs. 12(c) and 12(d)] and the discommensurate CDW state. Namely, if two possible directions of the V-V dimers in Figs. 12(c) and 12(d) are considered as the 0-phase state and the π-phase state in the CDW state, a V trimer acts as a domain wall with a π-phase shift. In this analogy, the increase in q with decreasing T below $T_{\mathrm{ic}\,ab} = 210$ K can be regarded as an increase in the number of the domain walls, and the threefold superstructure below T_{triple} corresponds the state with only the domain walls. We speculate that an effective attractive interaction between the domain walls (V trimers) is possibly the origin of such a behavior. This scenario means that various superstructures in $BaV_{10}O_{15}$ are based on the V trimer, which itself is a superstructure caused by the orbital ordering.

Since there is no magnetic ordering above $T_N = 43$ K in this compound, $\chi(T)$ shown in Fig. 4 is dominated by the spin-singlet state in the V trimer and the V dimer in this T range. For $T_s = 135\ \mathrm{K} < T < T_{\mathrm{triple}} = 176$ K [below the left triangle in Fig. 4(b)], all the V ions form trimers [Fig. 12(b)] whereas for $T_{\mathrm{ic}\,ab} = 210\ \mathrm{K} < T < T_{\mathrm{com}} = 240$ K [above the right triangle in Fig. 4(b)], all the V ions form dimers [see Figs. 12(c) and 12(d)]. From $T_{\mathrm{ic}\,ab} = 210$ K to $T_{\mathrm{triple}} = 176$ K [between the two triangles in Fig. 4(b)], the number of the V trimers increases whereas that of the V dimers decreases. Based on these scenario, $\chi(T)$ shown in Fig. 4(b), which is characterized by a larger slope between $T_{\mathrm{triple}} = 176$ K and $T_{\mathrm{ic}\,ab} = 210$ K, can be explained by a larger susceptibility of the V trimer than that of the V dimer by several percent, probably because of a smaller spin gap.

The phase transition at $T_s = 135$ K from the threefold superstructure [Fig. 12(b)] to the alternate arrangement of the V trimers and the lone V ions [Fig. 12(a)] can also be explained by the commensurability energy. Here, we point out that upon the first-order phase transition at $T_s = 135$ K, the entropy should decrease with decreasing T, resulting in the latent heat. Since the spin entropy is suppressed above T_s because of the singlet formation in the V trimers, the spin entropy of the lone V should also be suppressed below T_s, indicating a strong antiferromagnetic correlation (local antiferromagnetic ordering) below T_s even above $T_N = 43$ K in this compound.

Let us also consider the possible origin of the incommensurate peaks along the c axis between $T_{\mathrm{ic}\,c} = 250$ K and $T_{\mathrm{com}} = 240$ K shown in Fig. 9. As discussed in the introduc-

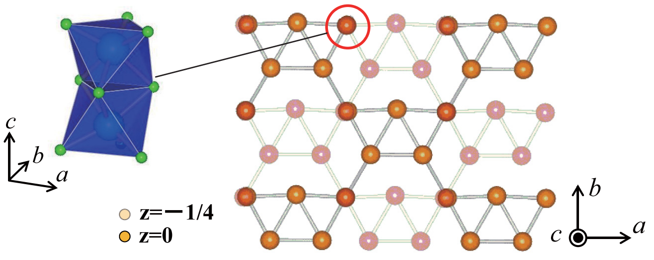

FIG. 13. Arrangement of the V ions in $BaV_{10}O_{15}$ along the *ab* plane in neighboring bilayers (light and dark colors), and the two VO_6 octahedra along the *c* axis, drawn using VESTA [36].

tion, V ions form a triangular lattice from which triangles are periodically missing along the *ab* plane [Fig. 1(a)], and two layers of this quasitriangular lattice are stacked as a bilayer slab of the fcc structure [Fig. 1(b)]. Here, one bilayer and the neighboring bilayer are shifted by $a/2$, where a is the lattice constant along the a axis, as shown in Fig. 13. As a result, V ions stack exactly above the V ions in the neighboring layer, where the two VO_6 octahedra along the c axis share a face, as shown in Fig. 13. According to a Hartree-Fock calculation, 2.5 electrons per V ion on average are distributed equally on this V dimer [46]. One possibility is that such a fractional number of electrons causes a modulation with a much longer period along the c axis in the real material.

V. SUMMARY

We studied $BaV_{10}O_{15}$ in which V ions with the average valence of 2.8 ($d^{2.2}$) form a quasitriangular lattice along the *ab* plane. In addition to the structural phase transition at $T_s = 135$ K, which is characterized by the alternate arrangement of V trimers caused by the V orbital ordering and lone V ions along the b axis, various ordered phases are found above T_s. Anomalies are observed in the resistivity, magnetic susceptibility, strain, and specific heat at $T_{\mathrm{triple}} = 175$ K and $T_{\mathrm{ic}\ ab} = 210$ K. According to the x-ray diffraction of the single crystal, ($qq0$)-type superstructures appear below $T_{\mathrm{ic}\ ab} = 210$ K, and q continuously increases with decreasing T and is locked to $1/3$ at $T_{\mathrm{triple}} = 175$ K. These superlattice peaks with $q = 1/3$, suggesting the threefold superstructure, are most likely caused by the dense arrangement of the V trimers along the zigzag double chain of the V ions along the b axis. The continuous change in q between $T_{\mathrm{triple}} = 175$ K and $T_{\mathrm{ic}\ ab} = 210$ K can be explained by the insertion of the V dimers between two V trimers. Such a change in q with T over one third of the Brillouin zone has rarely been observed in conventional charge-density-wave phases or charge-ordered phases and can be attributed to the peculiar characteristic of the superstructure of V trimers, each of which is also a superstructure. In addition to such superstructures along the *ab* plane, ($00q'$)-type superlattice peaks with $q' \sim 0.1$ appear below $T_{\mathrm{ic}\ c} = 250$ K and q' goes to 0 at $T_{\mathrm{com}} = 240$ K.

ACKNOWLEDGMENTS

We thank Y. Nagamine for his help with the electron diffraction measurement, and T. Okuda and T. Mizokawa for enlightening discussions. This work was supported by JSPS KAKENHI Grant No. 19H01853.

---

[1] J. A. Wilson, F. J. Di Salvo, and S. Mahajan, Charge-Density Waves in Metallic, Layered, Transition-Metal Dichalcogenides, Phys. Rev. Lett. **32**, 882 (1974).

[2] R. M. Fleming, F. J. DiSalvo, R. J. Cava, and J. V. Waszczak, Observation of charge-density waves in the cubic spinel structure CuV_2S_4, Phys. Rev. B **24**, 2850 (1981).

[3] M. H. Whangbo, Analogies between the concepts of molecular chemistry and solid-state physics concerning structural instabilities. electronic origin of the structural modulations in layered transition metal dichalcogenides, J. Am. Chem. Soc. **114**, 9587 (1992).

[4] S. Kawaguchi, H. Ishibashi, N. Tsuji, J. Kim, K. Kato, M. Takata, and Y. Kubota, Structural properties in incommensurately modulated spinel compound CuV_2S_4, J. Phys. Soc. Jpn. **82**, 064603 (2013).

[5] S. Ramakrishnan, A. Schönleber, C. B. Hübschle, C. Eisele, A. M. Schaller, T. Rekis, N. H. A. Bui, F. Feulner, S. van Smaalen, B. Bag, S. Ramakrishnan, M. Tolkiehn, and C. Paulmann, Charge density wave and lock-in transitions of CuV_2S_4, Phys. Rev. B **99**, 195140 (2019).

[6] S. Shimomura, C. Hayashi, G. Asaka, N. Wakabayashi, M. Mizumaki, and H. Onodera, Charge-Density-Wave Destruction and Ferromagnetic Order in $SmNiC_2$, Phys. Rev. Lett. **102**, 076404 (2009).

[7] S. Shimomura, C. Hayashi, N. Hanasaki, K. Ohnuma, Y. Kobayashi, H. Nakao, M. Mizumaki, and H. Onodera, Multiple charge density wave transitions in the antiferromagnets $RNiC_2$ ($R =$ Gd, Tb), Phys. Rev. B **93**, 165108 (2016).

[8] C. H. Chen, S.-W. Cheong, and A. S. Cooper, Charge Modulations in $La_{2-x}Sr_xNiO_{4+y}$: Ordering of Polarons, Phys. Rev. Lett. **71**, 2461 (1993).

[9] C. H. Chen, S. Mori, and S.-W. Cheong, Anomalous Melting Transition of the Charge-Ordered State in Manganites, Phys. Rev. Lett. **83**, 4792 (1999).

[10] T. Yamauchi, H. Ueda, K. Ohwada, H. Nakao, and Y. Ueda, Devil's staircase of odd-number charge order modulations in divalent β-vanadium bronzes under pressure, Phys. Rev. B **97**, 125138 (2018).

[11] E. Fawcett, Spin-density-wave antiferromagnetism in chromium, Rev. Mod. Phys. **60**, 209 (1988).

[12] Y. Ishikawa, K. Tajima, D. Bloch, and M. Roth, Helical spin structure in manganese silicide mnsi, Solid State Commun. **19**, 525 (1976).

[13] K. Wang, J.-M. Liu, and Z. Ren, Multiferroicity: the coupling between magnetic and polarization orders, Adv. Phys. **58**, 321 (2009).

[14] A. J. Millis, Lattice effects in magnetoresistive manganese perovskites, Nature (London) **392**, 147 (1998).

[15] Y. Tokura and N. Nagaosa, Orbital physics in transition-metal oxides, Science **288**, 462 (2000).

[16] M. Isobe, E. Ninomiya, A. N. Vasilév, and Y. Ueda, Novel phase transition in spin-1/2 linear chain systems: $NaTiSi_2O_6$ and $LiTiSi_2O_6$, J. Phys. Soc. Jpn. **71**, 1423 (2002).

[17] M. J. Konstantinović, J. van den Brink, Z. V. Popović, V. V. Moshchalkov, M. Isobe, and Y. Ueda, Orbital dimerization in $NaTiSi_2O_6$: An orbital analogue of the spin-peierls phase transition, Phys. Rev. B **69**, 020409(R) (2004).

[18] H. F. Pen, J. van den Brink, D. I. Khomskii, and G. A. Sawatzky, Orbital Ordering in a Two-Dimensional Triangular Lattice, Phys. Rev. Lett. **78**, 1323 (1997).

[19] T. Jin-no, Y. Shimizu, M. Itoh, S. Niitaka, and H. Takagi, Orbital reformation with vanadium trimerization in d^2 triangular lattice $LiVO_2$ revealed by ^{51}V NMR, Phys. Rev. B **87**, 075135 (2013).

[20] Y. Horibe, M. Shingu, K. Kurushima, H. Ishibashi, N. Ikeda, K. Kato, Y. Motome, N. Furukawa, S. Mori, and T. Katsufuji, Spontaneous Formation of Vanadium "Molecules" in A Geometrically Frustrated Crystal: AlV_2O_4, Phys. Rev. Lett. **96**, 086406 (2006).

[21] J. Miyazaki, K. Matsudaira, Y. Shimizu, M. Itoh, Y. Nagamine, S. Mori, J. E. Kim, K. Kato, M. Takata, and T. Katsufuji, Formation of a Three-Dimensional Network of v Trimers in $A_2V_{13}O_{22}$ (A = Ba, Sr), Phys. Rev. Lett. **104**, 207201 (2010).

[22] A. J. Browne, S. A. J. Kimber, and J. P. Attfield, Persistent three- and four-atom orbital molecules in the spinel AlV_2O_4, Phys. Rev. Materials **1**, 052003(R) (2017).

[23] T. Kajita, Y. Obata, Y. Kakesu, Y. Imai, Y. Shmizu, M. Itoh, H. Kuwahara, and T. Katsufuji, Trimerization and orbital ordering in $Ba_{1-x}Sr_xV_{13}O_{18}$, Phys. Rev. B **96**, 245126 (2017).

[24] A. E. Nikiforov, S. Y. Shashkin, M. L. Levitan, and T. H. Agamalyan, Cooperative jahn-teller orbital ordering in $KCuF_3$ and K_2CuF_4 crystals, Phys. Status Solidi B **118**, 419 (1983).

[25] P. Khalifah, R. Osborn, Q. Huang, H. W. Zandbergen, R. Jin, Y. Liu, D. Mandrus, and R. J. Cava, Orbital ordering transition in $La_4Ru_2O_{10}$, Science **297**, 2237 (2002).

[26] S. J. Moon, W. S. Choi, S. J. Kim, Y. S. Lee, P. G. Khalifah, D. Mandrus, and T. W. Noh, Orbital-Driven Electronic Structure Changes and the Resulting Optical Anisotropy of the Quasi-Two-Dimensional Spin Gap Compound $La_4Ru_2O_{10}$, Phys. Rev. Lett. **100**, 116404 (2008).

[27] Y. Miura, Y. Yasui, M. Sato, N. Igawa, and K. Kakurai, New-type phase transition of Li_2RuO_3 with honeycomb structure, J. Phys. Soc. of Jpn. **76**, 033705 (2007).

[28] J. P. Sheckelton, J. R. Neilson, D. G. Soltan, and T. M. McQueen, Possible valence-bond condensation in the frustrated cluster magnet $LiZn_2Mo_3O_8$, Nat. Mater. **11**, 493 (2012).

[29] G. Liu and J. Greedan, Structure and magnetism in $AB_{10}O_{15+x}$ (A = Sr, Ba; B = V, Cr; $x = 0 \sim 1$): Evidence for geometric frustration, J. Solid. State Chem. **122**, 416 (1996).

[30] C. A. Bridges and J. E. Greedan, Phase transitions and electrical transport in the mixed-valence V^{2+}/V^{3+} oxide $BaV_{10}O_{15}$, J. Solid State Chem. **177**, 1098 (2004).

[31] C. A. Bridges, J. E. Greedan, and H. Kleinke, Insights on the origin of the structural phase transition in $BaV_{10}O_{15}$ from electronic structure calculations and the effect of ti-doping on its structure and electrical transport properties, J. Solid State Chem. **177**, 4516 (2004).

[32] C. A. Bridges, T. Hansen, A. S. Wills, G. M. Luke, and J. E. Greedan, Frustrated magnetism and the effects of titanium substitution in the mixed-valence oxide $BaV_{10-x}Ti_xO_{15}$, Phys. Rev. B **74**, 024426 (2006).

[33] T. Kajita, T. Kanzaki, T. Suzuki, J. E. Kim, K. Kato, M. Takata, and T. Katsufuji, Opening of a charge gap with v trimerization in $BaV_{10}O_{15}$, Phys. Rev. B **81**, 060405(R) (2010).

[34] Y. Shimizu, K. Matsudaira, M. Itoh, T. Kajita, and T. Katsufuji, Spin-singlet trimer state induced by competing orbital order in triangular-lattice $BaV_{10}O_{15}$, Phys. Rev. B **84**, 064421 (2011).

[35] K. Takubo, T. Kanzaki, Y. Yamasaki, H. Nakao, Y. Murakami, T. Oguchi, and T. Katsufuji, Orbital states of v trimers in $BaV_{10}O_{15}$ detected by resonant x-ray scattering, Phys. Rev. B **86**, 085141 (2012).

[36] K. Momma and F. Izumi, VESTA3 for three-dimensional visualization of crystal, volumetric and morphology data, J. Appl. Crystallogr. **44**, 1272 (2011).

[37] T. Katsufuji, T. Okuda, R. Murata, T. Kanzaki, K. Takayama, and T. Kajita, Universal behaviors of the phonon thermal conductivity associated with charge/orbital ordering in transition-metal oxides, J. Phys. Soc. Jpn. **85**, 013703 (2016).

[38] M. Marezio, D. B. McWhan, J. P. Remeika, and P. D. Dernier, Structural aspects of the metal-insulator transitions in Cr-doped VO_2, Phys. Rev. B **5**, 2541 (1972).

[39] P. J. Hsu, T. Mauerer, M. Vogt, J. J. Yang, Y. S. Oh, S.-W. Cheong, M. Bode, and W. Wu, Hysteretic Melting Transition of A Soliton Lattice in a Commensurate Charge Modulation, Phys. Rev. Lett. **111**, 266401 (2013).

[40] M. Hoshino, T. Kajita, T. Kanzaki, M. Uchida, Y. Tokura, and T. Katsufuji, Charge-gap formation in the insulating states of $AV_{10}O_{15}$ (A = Ba, Sr), Phys. Rev. B **85**, 085106 (2012).

[41] T. Saiki, S. Ohkubo, K. Funahashi, T. Yamazaki, T. Kajita, and T. Katsufuji, Change in the optical spectrum of $BaV_{10}O_{15}$ with applied uniaxial strain, Phys. Rev. B **101**, 121111(R) (2020).

[42] J. A. Wilson, F. J. DiSalvo, and S. Mahajan, Charge-density waves and superlattices in the metallic layered transition metal dichalcogenides, Adv. Phys. **24**, 117 (1975).

[43] D. E. Moncton, J. D. Axe, and F. J. DiSalvo, Study of Superlattice Formation in 2H-$NbSe_2$ and 2H-$TaSe_2$ by Neutron Scattering, Phys. Rev. Lett. **34**, 734 (1975).

[44] W. L. McMillan, Theory of discommensurations and the commensurate-incommensurate charge-density-wave phase transition, Phys. Rev. B **14**, 1496 (1976).

[45] K. Nakanishi and H. Shiba, Domain-like incommensurate charge-density-wave states and the first-order incommensurate-commensurate transitions in layered tantalum dichalcogenides. II. 2H-polytype, J. Phys. Soc. Jpn. **44**, 1465 (1978).

[46] T. Yoshino, M. Okawa, T. Kajita, S. Dash, R. Shimoyama, K. Takahashi, Y. Takahashi, R. Takayanagi, T. Saitoh, D. Ootsuki, T. Yoshida, E. Ikenaga, N. L. Saini, T. Katsufuji, and T. Mizokawa, Unusual valence state and metal-insulator transition in $BaV_{10}O_{15}$ probed by hard x-ray photoemission spectroscopy, Phys. Rev. B **95**, 075151 (2017).